AAS 17-756

CELL-MAPPING ORBIT SEARCH FOR MISSION DESIGN AT OCEAN WORLDS USING PARALLEL COMPUTING

Dayung Koh,* Rodney L. Anderson,† and Ivan Bermejo-Moreno‡

In this study, a cell-mapping approach is applied to various systems in the circular restricted three-body problem to obtain a rapid understanding of the global dynamics. The method is generic for various classes of problems including non-autonomous systems and different types of periodic solutions. The cell-mapping method also does not require previously known solutions as inputs, which is typical of continuation approaches, and no symmetric constraints are imposed. This method is especially applicable to a systematic periodic orbit search over a region of interest at one-period of integration. As additional strengths of the method, multiple-period solutions and bifurcation studies can be easily performed. In this study, the initial orbit search is applied to obtain an understanding of the orbit trade space at Europa and Enceladus.

INTRODUCTION

Poincaré[1] considered periodic orbits to be key to understanding the nonlinear dynamics in the three-body problem. The computation of periodic orbits in the three-body problem has since been approached by many researchers in celestial mechanics and astrodynamics. The majority of these studies have focused on the autonomous circular restricted three-body problem (CRTBP) using a variety of models and methods. Much of the early analytical work and numerical explorations by researchers such as Strömgren, Darwin, and Moulton are summarized nicely by Szebehely[2] who broadly refers to these investigations as the Copenhagen category. He also discusses other periodic orbit work, along with the particular models that were used, up through the mid-1960s. Much of this work and even that of later researchers are focused on specific mass ratios or models. We are concerned primarily here with developing a method to perform thorough initial explorations of new systems or models as they become relevant for particular astrodynamics or celestial mechanics problems. A key component of the search in these cases is often to be able to perform it in a short time-frame using a method that can be applied to a generic dynamical system.

More recent numerical methods for a selected set of studies are summarized in the following as well as in Table 1. Although by no means comprehensive, this list of references gives an idea of the favored methodologies for approaching this problem. A simple 'predictor - corrector' procedure was used in many numerical computation techniques. For this method, an initial guess is selected and an iteration process is used until convergence to a periodic orbit. Goudas,[3] Markellos,[4] Zagouras and Markellos,[5] Robin and Markellos,[6] Zagouras,[7] and Howell[8] are just some of the researchers that have used this method.

There are two important components of the procedure: how to select the initial guess and how to compute periodic solutions. In many of these studies, initial conditions for the search space were determined with points emanating from the libration points or planar symmetric periodic orbits known from the previous results. Goudas[3] computed three-dimensional periodic orbit families (all are doubly symmetric) which were an extension of Moulton's family around the collinear libration points. Markellos[4] studied two-dimensional symmetric periodic orbits in the Sun-Jupiter (S - J) system as branches of a given family of orbits. Hénon[9] focused on out-of-plane perturbations of plane periodic orbits and evaluated the 'vertical stability index' for

*Postdoctoral Fellow, Jet Propulsion Laboratory, California Institute of Technology, USA, Dayung.Koh@jpl.nasa.go
†Member of Technical Staff, Jet Propulsion Laboratory, California Institute of Technology, USA, Rodney.L.Anderson@jpl.nasa.gov
‡Assistant Professor, Aerospace and Mechanical Engineering Department, University of Southern California

the specified planar orbit family. Zagouras and Markellos[5] and Robin and Markellos[6] examined the stability index for the S - J system and studied the bifurcated symmetric vertical critical orbits which emanated from members of the planar families. Zagouras[7] located the initial conditions at the triangular libration points and computed symmetric periodic solutions using fourth-order parametric expansions. A second family of non-symmetric periodic orbits was then found to bifurcate from the symmetric orbits. Howell[8] studied quasi-periodic orbits associated with the approximately computed analytic solutions around the collinear libration points.

Table 1: Numerical computation methods of periodic solutions of the CRTBP

Author(year)	mass parameter	Initial Conditions	Convergence	Dimension	Symmetricity
Goudas (1963)[3]	0.1- 0.5	equilibrium pts, planar families	perturbation	three	sym
Message (1970)[10]	0.00095 (S-J)	Von Ziepel's transformation	perturbation	two	asym
Farquhar (1973)[11]	1/82.30 (E-M)	Linearized motion around L_2	Lindstedt-Poincare method	three	sym
Markellos (1974)[12]	0 - 0.5	grid (x_0,0,0,$\dot{y}_0$)	scanning	two	sym
Kazantzis (1975)[13]	0.4	grid (x_0,0,0,0,$\dot{y}_0$,$\dot{z}_0$)	differential corrector	three	sym
Markellos (1978)[14]	0.45	Planar sym. orbits	differential corrector	three	asym
Robin (1979)[6]	0.00095 (S-J)	Retrograde planar symmetric orbits	differential corrector	three	sym
Breakwell (1979)[16]	1/82.30 (E-M)	Farquhar(1973)[11] solutions	differential corrector (single shooting)	three	sym
Howell (1984)[17]	0 - 1	Breakwell(1979)[16] results	differential corrector (single shooting)	three	sym
Zagouras (1985)[7]	0.00095 (S-J)	symmetric orbits and $L_{4,5}$	analytic solutions/ perturbation	three	sym,asym
Howell (1988)[8]	3.04e-06, 0.012	analytic approximations	differential corrector (multiple shooting)	three	sym
Hénon (2003)[18]	Hill's problem	grid	differential corrector	two	sym
Papadakis (2008)[20]	0 - 0.5	symmetric orbits and $L_{1,2,3}$	differential corrector	three	asym

As implied above, the computed periodic orbits were symmetric in the majority of these studies (with various combinations of symmetries). The reason is that the periodic solutions were found with a set of initial conditions as introduced above, but in such a manner that the mirror configuration is preserved.[15] The conditions are described uniquely by the type of symmetry involved (axi, plane, doubly-symmetry, etc.). Then the initial condition is parametrically continued to compute periodic solutions using differential correctors. In particular, refer to Farquhar[21] for an explanation of a typical single-shooting method and Wilson[22] for a multiple-shooting method.

It was claimed that greater complexity in the numerical procedures and a large amount of computing effort are required to continue a family of asymmetric periodic solutions compared to symmetric ones.[23] Some of the asymmetric periodic solutions are discussed in Message,[10] Markellos,[14] Taylor,[23] and Papadakis.[20] In each case, they utilized bifurcations from planar symmetric periodic orbits to continue the families.

Grid search methods were introduced in order to facilitate the calculation by Markellos et al.,[12] Kazantiz and Goudas,[13] Hénon,[18] and Tsirogiannis et al.,[19] yet they used the same symmetric periodic orbit scanning procedure as before. Either two-dimensional or three-dimensional grid searches were applied to locate the initial conditions with a symmetric configuration, and they are integrated then until they met the symmetry configuration next. The procedure repeats throughout a grid of initial conditions and/or energy constants, one by one. (This will be compared to the proposed method.) Russell[27] successfully computed a number of families of periodic orbits in Jupiter-Europa system with a grid and various symmetry conditions.

These approaches were able to capture various periodic solutions and give some of the answers to how they were generated from other orbits. The periodic orbits of the CRTBP have been recognized to be valuable in real-world science missions and space exploration[24] in addition to their mathematical interest. However, the methods for computing periodic solutions have generally been limited by several constraints. At least one of the following has to be known: 1) a natural origin (equilibrium point), 2) pre-known solution branches, or 3) a stability index of solutions to indicate bifurcations. Moreover, most previous studies are based on symmetric configurations which require a particular setup to compute periodic orbits. Therefore it becomes challenging to explore undiscovered systems or the global system behavior.

In this study, the cell-mapping method was applied to different multi-body problems for orbit searches

that would be difficult to study using existing methods. The cell-mapping method was established by Hsu[25] for numerical determination of the global behavior of nonlinear dynamic systems. The concept of defining a confined state space and setting a grid to investigate the dynamics is similar to various grid search methods.[12,13,20,27] The cell-mapping method differs from these methods in that it links the grid throughout the state space we have selected by one period of integration, which together with unravelling methods, provides additional insight into broader periodic motions. The period can be any value for a Hamiltonian system, but it is important to choose a fundamental period or a fraction of it. The dynamic behavior in the state space can then be analyzed and visualized. One of the extensions of the cell-mapping method, set-oriented methods, has been developed to improve the accuracy of the invariant solutions with subdivision techniques.[28–30] We are focused here though on developing a methodology for the full global dynamical behavior with the rapid exploration of new systems or known systems with new parameters. The ability to focus this search on orbits with particular periods is also beneficial as this is often a key constraint for many mission design scenarios.

To summarize the main features of the cell-mapping method:

1. It is generic, open to any type of system, any configuration of periodic orbits, and any system dimension. No special care (such as symmetry conditions) for different types of orbits is required.

2. It pre-filters solutions before going through differential correction, i.e. saves computation by filtering duplicates out.

3. Once a 'cell-map' is found, periodic orbits as well as multiple-periodic solutions (and attractors) can be determined.

4. For mission design applications, all the periodic solutions could be computed in a particular region of interest with a defined period.

This approach has been successfully applied to a wide range of problems. The method was used for planning optimum trajectories of multiple robot arms by Wang and Lever,[31] analyzing the pitch motion of a gravity gradient satellite in elliptic orbits by Koh and Flashner,[32] and studying coupled orbit-attitude dynamics in the elliptic three-body problem by Koh and Anderson.[33] Ding et al.[34] investigated the global behavior including limit cycle oscillation, periodic motions, and domains of attraction of a bilinear stiffness aeroelastic system by an improved cell-mapping method.

MOTIVATION FOR USING CELL MAPPING WITH PARALLEL COMPUTING

Historically, cell-mapping methods have been used to obtain a global overview of periodic solutions in a given dynamical system. Limitations in computing resources made it difficult to apply these methods to higher dimensional problems such as the CRTBP, and most of the initial work focused on lower dimensional problems.[25] Cell-mapping methods do, however, offer some advantages over other methods currently in use for searching for periodic orbits in the CRTBP such as continuation and various grid search methods in combination with single-shooting techniques. Most notably, cell-mapping methods automatically provide n-periodic solutions when orbits of a given period are computed, and they are able to find asymmetric periodic orbits as easily as symmetric ones. Recent advances in computing have made it more feasible to use cell-mapping methods in the CRTBP and take advantage of the benefits of the cell mapping approach.

One of the primary motivations of the current work is to be able to quickly obtain a general overview of the periodic orbits of a new system when a new mission or scientific objective is proposed. In other words, while a particular system may have been analyzed in significant detail via continuation or single shooting, when a new mission is proposed to a new system, the periodic orbits need to be recomputed. If the model relevant for that particular system is of the same type, then continuation may be required for each of the families. This tedious process may be possible for some models that are similar, but it requires knowledge of the families and how they may bifurcate with the relevant parameters. If the model for the new system is of a significantly different type, these continuation methods may not be feasible, and in that case equilibrium

points and continuation from these points would need to be started from scratch. In this case, cell-mapping methods are more attractive for obtaining an initial overview of the periodic orbits in the new problem.

This study lays the foundation for this general approach to obtain a general overview of the periodic orbits of a system which may involve a new type of model, such as the augmented Hills three-body problem relevant for asteroids.[35,36] Given the instabilities present in the CRTBP compared to previous applications,[33] some challenges do exist in terms of the grid necessary to capture the periodic orbits of interest in this problem and other parameters. In this study, these challenges are addressed, and cell-mapping methods are applied to some of the icy moon systems of current interest.[37]

METHODOLOGY

In this section, the cell-mapping method of Hsu[25,26] is briefly described. A more detailed explanation of the approach used here may be found in Koh and Anderson[33] and Koh.[38] In the final subsection, the computational approach is summarized.

Cell mapping formulation

Consider a dynamical system

$$\dot{\boldsymbol{x}}(t) = f(t, \boldsymbol{x}(t)) \tag{1}$$

and define the states x_i, $i = 1, 2, ..., N$ (N=number of states) to get a state representation. The cell state space S is constructed by dividing the bounded state variables between $x_i^{(L)}$ (lower limit) and $x_i^{(U)}$ (upper limit) into a small interval with uniform size h_i. Each cell center is considered to be an entity represented by an integer, and the state space S is regarded as a collection of these cells. The region outside of this bounded region is defined as the 'sink cell.'

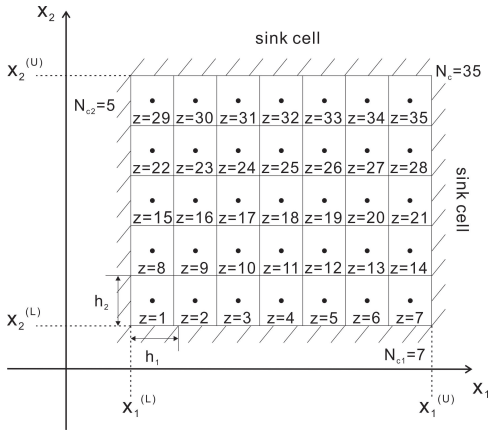

Figure 1: Cell state space for $N = 2$

Figure 1 presents an example for a two dimensional system. Each state variable, x_1 and x_2, is divided into a finite number of cells, N_{c1} and N_{c2}, with intervals of h_1 and h_2, respectively. Then S contains a total number of cells $N_c = N_{c_1} \times N_{c_2}$. Each cell is identified by its center point and numbered sequentially, $z = 1$ to $z = N_c$. In the cell state space S, one can form the cell-mapping C of a dynamical system by integrating it for one specified period T. The evolution of a discrete dynamical system can be described by

$$z(n+1) = C(z(n)) \tag{2}$$

where $C : S \to S,\ z(n) = 1, 2, \cdots, N_c$. Refer to Koh and Anderson[33] for an example of a schematic cell mapping with the cell state space. Cells numbered from $z = 1$ to $z = 35$ are mapped to $C(z)$ after one integration of period T.

Computation of discrete periodic solutions

Once the mapping process is complete, i.e., we have $C(z)$, the properties of the cells are determined using an unraveling algorithm (see Hsu[26]). The dynamics of the cell mapping is characterized by classifying singular cells as either equilibrium cells or periodic cells. An equilibrium (or period one) cell z^* is given by

$$z^* = C^1(z^*). \tag{3}$$

To define periodic cells, let C^m denote the cell-mapping C applied m times (m is an integer) with C^0 understood to be the identity mapping. A sequence of K distinct cells $z^*(j)$, $j = 1, 2, \cdots, K$ which satisfies

$$\begin{aligned} z^*(m+1) &= C^m(z^*(1)),\ m = 1, 2, \cdots, K-1, \\ z^*(1) &= C^K(z^*(1)) \end{aligned} \tag{4}$$

is a $P - K$ mapping.

To delineate the global properties, three entities are defined from the unraveling algorithm, as follows:

1. Group number (Gr): Positive integers that are assigned sequentially as the periodic motions are discovered. Each group has an invariant set in the form of a periodic motion and shares the same periodicity number.
2. Periodicity number (P): This number indicates that the cell or the periodic motion of a group that the cell belongs to is periodic with period of $P \cdot T$.
3. Step number (S): The number of steps to map a cell into a group is assigned to each cell. If the step number of z is 0, it is a periodic cell.

Figure 2 shows the $P - 1$ and $P - 3$ periodic cells as an example. The hashed cell is an equilibrium ($P - 1$) cell which maps back to itself after one period. The dotted cells are $P - 3$ cells where each one of them maps back to the same cell after three periods. A detailed example can be found in Koh and Anderson.[33]

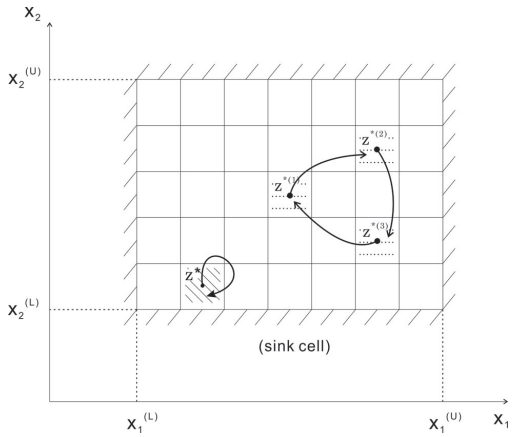

Figure 2: Equilibrium cell z^* and $P - K$ cells $z^{*(i)},\ i = 1, \cdots,\ K$ for $K = 3$

Solution refinement via differential corrector

A multiple-shooting differential correction algorithm[22] is adopted in order to find an exact periodic solution $\boldsymbol{x}^*$ from the discrete periodic solutions. Specifically, a two-step iterative process is implemented: 1) velocity adjustments at each patchpoint to perform a continuous trajectory. 2) position and epoch adjustments to reduce the total ΔV. Refer to Parker and Anderson[41] for details.

Stability and bifurcation conditions

After finding a periodic solution $\boldsymbol{x}^*$, its local stability can be investigated using eigenvalues of the monodromy matrix. Let us define $\boldsymbol{u}(t) = \boldsymbol{x}(t) - \boldsymbol{x}^*(t;\boldsymbol{s})$ as the perturbation of the state $\boldsymbol{x}$ about a periodic solution $\boldsymbol{x}^*$. In order to analyze the stability of the periodic solution, the first order Taylor series was taken from the system Eq. (1) as

$$\dot{\boldsymbol{u}}(t) = \boldsymbol{A}(t,\boldsymbol{s})\boldsymbol{u}(t) + \sum_{k=2}^{\infty} \boldsymbol{r}_k(t,\boldsymbol{u}(t),\boldsymbol{s};\boldsymbol{x}^*), \tag{5}$$

where the matrix $\boldsymbol{A}(t) \in \boldsymbol{R}^{N\times N}$ is given by

$$\boldsymbol{A}(t,\boldsymbol{s}) = \left[\frac{\partial \boldsymbol{f}(t,\boldsymbol{x},\boldsymbol{s})}{\partial \boldsymbol{x}}\right]_{x=x^*},$$

and $\boldsymbol{r}_k(t,\boldsymbol{u}(t),\boldsymbol{s};\boldsymbol{x}^*)$ is a vector of all polynomials of degree k in the components of $\boldsymbol{u}(t)$.

Then a discrete-time representation expressed by time-invariant difference equations (see[39,40]) can be obtained as

$$\boldsymbol{u}_{m+1} = \boldsymbol{H}(\boldsymbol{s})\boldsymbol{u}_m + h.o.t,\ m = 1,2,\cdots \tag{6}$$

where $H(\boldsymbol{s}) \in \boldsymbol{R}^{N\times N}$ is given by

$$\boldsymbol{H}(\boldsymbol{s}) = \boldsymbol{H}_K(\boldsymbol{s})\boldsymbol{H}_{K-1}(\boldsymbol{s})\cdots\boldsymbol{H}_1(\boldsymbol{s}). \tag{7}$$

Note that $\boldsymbol{H}(\boldsymbol{s})$ can be computed using an algorithm for computation of point mapping.[39,40]

The local stability of a $P-K$ solution is determined by the eigenvalues of monodromy matrix, $\boldsymbol{H}(\boldsymbol{s})$. Note that for Hamiltonian systems, $\boldsymbol{H}$ is symplectic, i.e., $det\boldsymbol{H}(\boldsymbol{s}) = 1$, and all eigenvalues of $\boldsymbol{H}$ satisfy $\lambda_{i+1}(\boldsymbol{H}) = 1/\lambda_i(\boldsymbol{H})$. When the eigenvalues of $\boldsymbol{H}$ reside on the unit circle, the solution is locally stable. If not, the solution is unstable with the pairs of eigenvalues satisfying $|\lambda_i(\boldsymbol{H})| > 1$ and $|\lambda_{i+1}(\boldsymbol{H})| < 1$.

Bifurcation from a $P-K$ solution to a $P-MK$ solution may occur if there exists an integer M such that

$$det(\boldsymbol{I} - \boldsymbol{H}^M) = 0 \tag{8}$$

(see[39]). In particular, one of the eigenvalues of $\boldsymbol{H}$ is $\lambda_{i,i+1} = 1$ for a $P-1$ to $P-1$ bifurcation, and $\lambda_{i.i+1} = -1$ for a $P-1$ to $P-2$ bifurcation.

Parallel Cell mapping implementation

For the global analysis of the nonlinear dynamic system, the cell-mapping method is utilized. Two main steps for the global analysis are developed. First, the cell mapping is obtained for the given dynamical system by integrating over one desired period T. Then, the global properties, such as equilibrium points, multiple-period periodic solutions, and regions of attraction of the system are extracted by an unraveling algorithm.

The computational algorithm is written using the C++ programming language and parallelized using the Message Passing Interface (MPI) for distributed computing on high performance computing (HPC) clusters. A procedure for the study is summarized in the following.

1. Select a cell state space and divide it into a finite number of cells as in Fig. 1
2. Develop a cell-mapping for the state space, see Eq. (2). The cell mapping in principle could be done independently for each cell, and is therefore fully parallelizable and scalable.
3. Employ the unraveling algorithm (see Hsu[26]) to analyze global properties, see Fig. 2. The unraveling algorithm presents the main challenge for parallelization as it requires collective (MPI Allreduce) and point-to-point communications (MPI Send, MPI Recv), but it is also parallelizable.
4. Find converged exact solution using differential correctors[21,22] as needed
5. Evaluate the local stability characteristics and bifurcation conditions of each solution using eigenvalues of the monodromy matrix of Eq. (7)

DESCRIPTION OF THE PROBLEM

Circular restricted three-body problem model

The CRTBP shown in Fig. 3 describes the motion of an infinitesimal mass with two primaries (e.g. the Earth and the Moon) under mutual gravitational attraction. A dimensionless rotating coordinate system ($X^R - Y^R - Z^R$) is defined at the barycenter of the two primaries with respect to the inertial frame ($X^I - Y^I - Z^I$), rotating about Z^I with true anomaly ν.

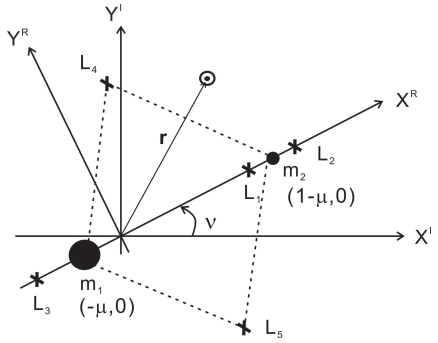

Figure 3: A schematic CRTBP configuration showing $x_1 = m_1$, $x_2 = m_2$, and the libration points in a non-dimensional rotating coordinate system $X^R - Y^R$, $Z^R(Z^I)$ are in the out-of-plane direction

The $X - axis$ of the rotating coordinate system is aligned with the vector from the larger primary body (m_1) to the second primary body (m_2), the $Z - axis$ is perpendicular to the primaries' orbital plane, and the $Y - axis$ completes the right-handed coordinate system. The position vector $\mathbf{r}$ points from the barycenter to the spacecraft in the rotating frame. The non-dimensional mass of the second primary is defined as μ and the larger body's mass as 1-μ (The Jupiter-Europa system: μ=2.5266448850435e-05, the Saturn-Enceladus system: μ=1.9002485658670e-07.)

Define the unit of time so that mean motion of the primary orbit is $n = 1$ (see Szebehely[2]). Then the equation of motion for the infinitesimal mass is written as

$$\begin{aligned}
\ddot{x} &= 2\dot{y} + x - (1-\mu)\frac{x+\mu}{r_1^3} - \mu\frac{x-1+\mu}{r_2^3} \\
\ddot{y} &= -2\dot{x} + y - (1-\mu)\frac{y}{r_1^3} - \mu\frac{y}{r_2^3} \\
\ddot{z} &= -(1-\mu)\frac{z}{r_1^3} - \mu\frac{z}{r_2^3}
\end{aligned} \tag{9}$$

where $r_1^2 = (x+\mu)^2 + y^2 + z^2$, $r_2^2 = (x-1+\mu)^2 + y^2 + z^2$. No closed form general solution is possible for the model. The Jacobi constant C is defined as

$$C = 2\Omega - V^2 = x^2 + y^2 + \frac{2(1-\mu)}{r_1} + \frac{2\mu}{r_2} - \dot{x}^2 - \dot{y}^2 - \dot{z}^2 \tag{10}$$

where the function Ω (effective potential) has the appearance of potential energy, and V is the magnitude of the velocity.

CELL MAPPING SETTING

To make effective use of the cell-mapping method, it is important to select an appropriate grid for each system and particular situation. Typically, the grid setting depends on the system's properties and users' interest for particular missions. The grid settings that we chose for this study are shown in Table 2.

Note that various other combinations of grid settings were tested; depending on the grid size, the cell mapping required between ten minutes and a couple of hours using eight-processors with a 64 MPI processes compute node. A tighter grid was required to capture orbit families for the smaller moon, Enceladus.

One of the state vector components was chosen to be fixed for implementing the cell mapping algorithm to reduce redundant outcomes and moderate the computation cost. The position x and the velocity x for the Jupiter-Europa system and the Saturn-Enceladus system, respectively, were chosen to show that fixing one component does not limit the result to particular families.

Table 2: Cell state space settings

Jupiter – Europa	x	y	z	$\dot{x}$	$\dot{y}$	$\dot{z}$
Upper Limit:	1-μ	0.02	0.12	0.07	0.07	0.03
Lower Limit:	1-μ	-0.02	-0.02	-0.07	-0.07	-0.03
grid size	0	0.004	0.004	0.004	0.004	0.004
Saturn – Enceladus	x	y	z	$\dot{x}$	$\dot{y}$	$\dot{z}$
Upper Limit:	1.0117	0.0074	0.0074	0	0.011	0.011
Lower Limit:	1.0005	-0.015	-0.015	0	-0.021	-0.021
grid size	0.0007	0.0007	0.0007	0	0.001	0.001

H_2 FAMILY ORBIT

The Jupiter-Europa (J-E) and Saturn-Enceladus (S-E) H_2 families which were computed using the cell-mapping method are presented in Fig. 4. Note that the H_2 family was computed using a shooting method search for symmetric orbits and published by Broucke.[42] Multiple mapping procedures for different periods were performed around the moons, and some of them from the cell mapping results were selected to present in this paper. As shown in Figure 4, there are orbits with similar shapes around the secondary with different

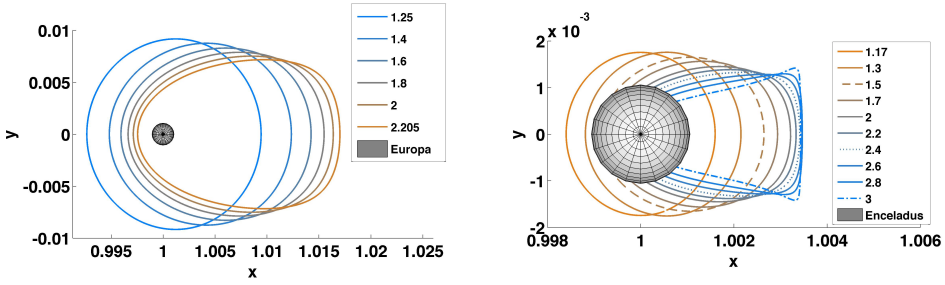

(a) Jupiter-Europa, period from 1.25 to 2.205

(b) Saturn-Enceladus, period from 1.17 to 3

Figure 4: Different period H_2 family

scales. Both systems have shorter period circular-shaped orbits, and they translate to relatively larger period egg-shaped orbits as the period increases. However, the size of the orbits is noticeably different. Comparable solutions around the smaller moon, Enceladus, are much closer to the surface than the ones around Europa.

H_2 P-1 orbit study

The H_2 orbits for the J-E and S-E systems are studied in more detail for potential missions for landers. This orbit family is interesting for potential use as relay-orbits because the orbits are stable and have visibility for particular landing sites. The H_2 family for varying Jacobi constant (C) or non-dimensional orbital period (T) is shown in Figures 5 and 6 for the J-E and S-E systems, respectively. As the period becomes longer and

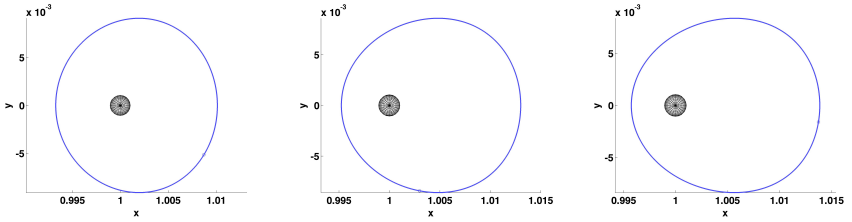

(a) C=3.00374495, T=1.27 (b) C=3.003670005, T=1.46 (c) C=3.003644741, T=1.555

(d) C=3.003626081, T=1.645 (e) C=3.003606483, T=1.77 (f) C=3.003568947, T=2.205

Figure 5: H_2 family of the J-E system, $1.25 < T < 2.21$

the Jacobi constant becomes smaller, the orbit becomes more elongated and egg-shaped for both systems. However, Enceladus orbits are much smaller in size, and they impact the surface quickly. Note that there is a mirrored family to the left side. The relay orbit can benefit from these stable family solutions in terms of reducing the risk of unexpected loss and mission cost, however, these orbits have limited visibility near the equator.

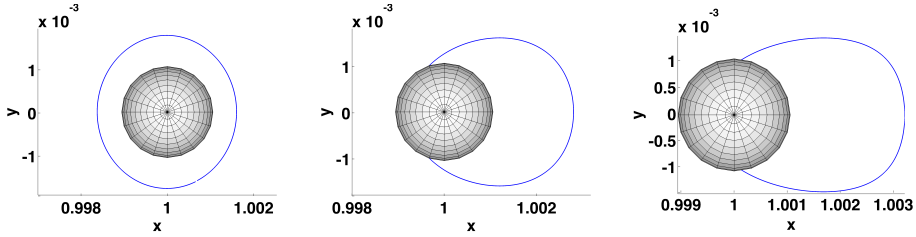

(a) C=3.000149103, T=1.2 (b) C=3.000142962, T=1.6 (c) C=3.000141052, T=2

Figure 6: H_2 family of the S-E system, $1.17 < T < 2$

The P-1 solution's stability characteristics for the two systems are similar to each other. Figure 7 shows the maximum eigenvalues for each orbit. Figures 7a and 7b show 'C - 3.00' vs. the maximum eigenvalues. The range of Jacobi constant for the S-E system for the same family orbit is smaller than the J-E system, but the stability characteristic tendency seems the same. Figure 7c shows the maximum eigenvalues vs. the period of the orbits. The size of orbits is scaled with respect to the size of the moon, but the stability characteristics are almost the same for both systems for the same dimensionless period orbits.

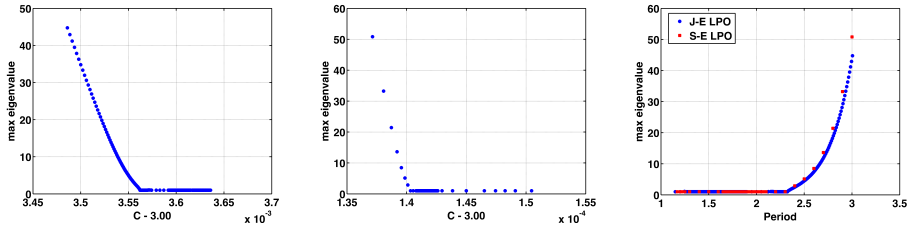

(a) Jupiter-Europa (b) Saturn-Enceladus (c) Both

Figure 7: H_2 family's maximum eigenvalue

H_2 family bifurcation study

Some of the multiple-period H_2 family solutions were found using the cell-mapping method. The x-y projection of the orbits and the Jacobi constant are close to those of the planar H_2 orbits, but the period of the solutions are doubled or tripled. A bifurcation study for this family was performed for both systems, and the

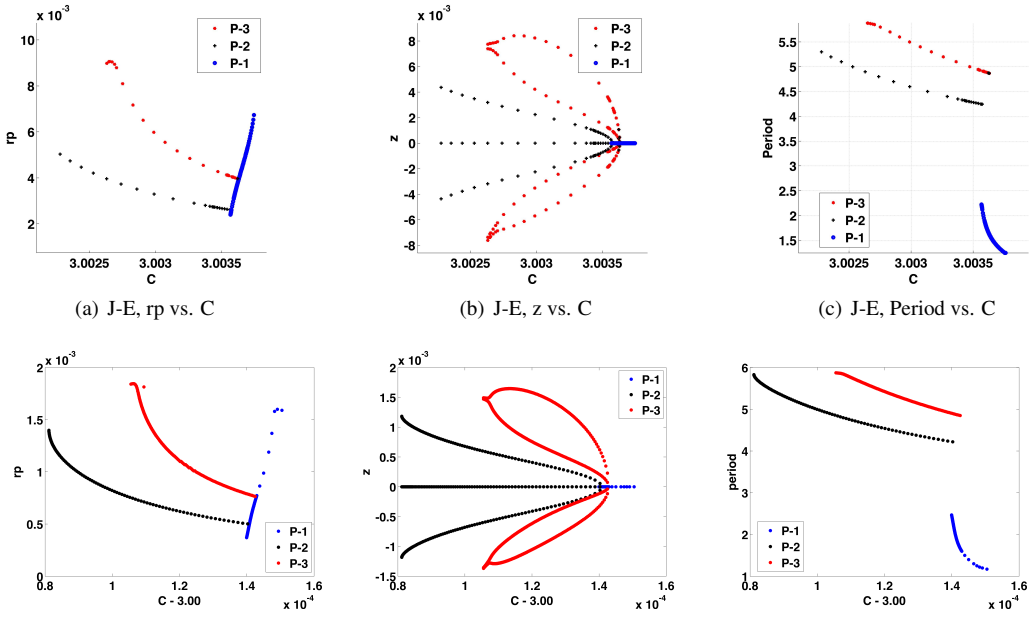

(a) J-E, rp vs. C (b) J-E, z vs. C (c) J-E, Period vs. C

(d) S-E, rp vs. 'C - 3.000' (e) S-E, z vs. 'C - 3.000' (f) S-E, Period vs. 'C - 3.000'

Figure 8: Bifurcation diagram of H_2 family

bifurcation diagram is shown in Fig. 8. Three projection views were chosen, the closest distance vs. C (Figs. 8a,d), the maximum z altitude when y = 0 vs. C (Figs. 8b,e), and period vs. C (Figs. 8c,f). Note that C - 3.000 was chosen as the x-axis for S-E to visualize the data better.

In common for both systems, P-2 and P-3 families that branched from the P-1 planar family can be seen from any projection in Fig. 8. The period jumps in the J-E system from T = 2.12175 to T = 4.2435 at C = 3.003574124 (P-1 to P-2) and T = 1.621666667 to T = 4.868859 at C = 3.003630499 (P-1 to P-3) are shown in Figure 8c. The period jumps in the S-E system from T = 2.1 to T = 4.2 at C = 3.000140783 (P-1 to P-2) and T= 1.6066667 to T = 4.82 at C = 3.000142912 (P-1 to P-3) are shown in Figure 8f.

The bifurcations can be verified with eigenvalues as well. Since the bifurcation diagrams are analogous to one another, the J-E case was chosen as an example. In Fig. 9, the eigenvalue indicator is presented vs. C. It is shown that $\lambda + 1/\lambda = -2$ for period doubling and $\lambda + 1/\lambda = -1$ for period tripling.

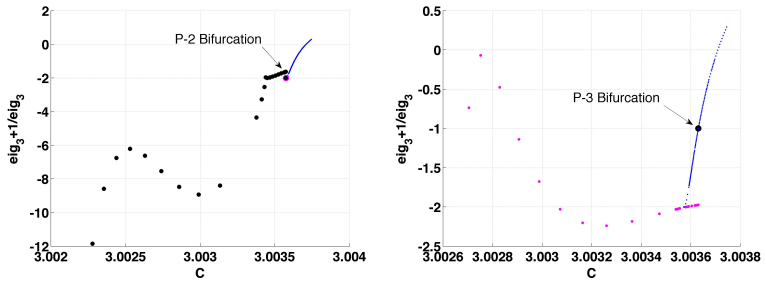

(a) P-1 to P-2 bifurcation (b) P-1 to P-3 bifurcation

Figure 9: Eigenvalue analysis for bifurcation of H_2 family for J-E

Another noteworthy result in the eigenvalue analysis is that the stability changes for bifurcated solutions. The stable H_2 P-1 family bifurcates to the H_2 P-2 family and becomes unstable whereas the bifurcated H_2 P-2 orbit is stable. The eigenvalue of the stable H_2 P-2 family crosses $\lambda + 1/\lambda = -2$ again and becomes unstable at C = 3.003439431. However, the H_2 P-3 family bifurcation is different. Both P-1 and P-3 are stable right after the bifurcation point. As C decreases from C = 3.003628817 to C = 3.00263168, the stable H_2 P-3 family becomes unstable at C = 3.003579142, and becomes stable again at C = 3.002987747. Then, highly inclined P-3 solutions for C $\lesssim$ 3.002987747 are stable. The maximum eigenvalues for both Europa and Enceladus H_2 P-3 families are shown in Fig. 10, and some selected orbits are shown in Figs. 11 and 12.

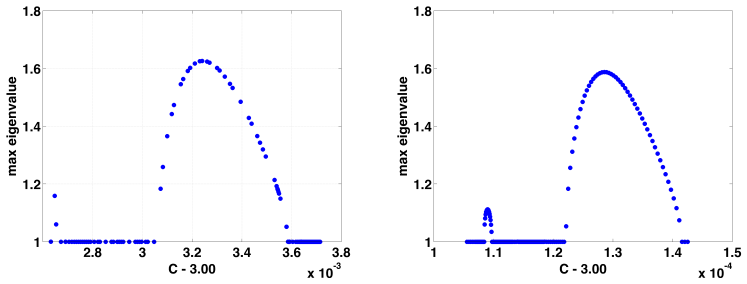

(a) Europa (b) Enceladus

Figure 10: H_2 P-3 family's maximum eigenvalue vs C

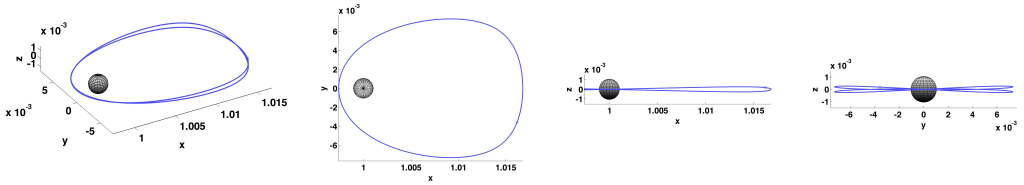

(a) P-2: C=3.00357374, T=4.244 (b) x-y (c) x-z (d) y-z, stable

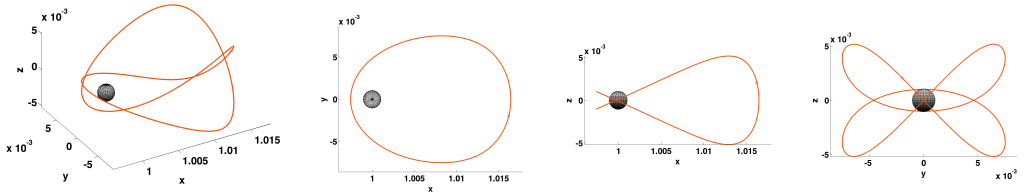

(e) P-2: C=3.003430357, T=4.32 (f) x-y (g) x-z (h) y-z, unstable

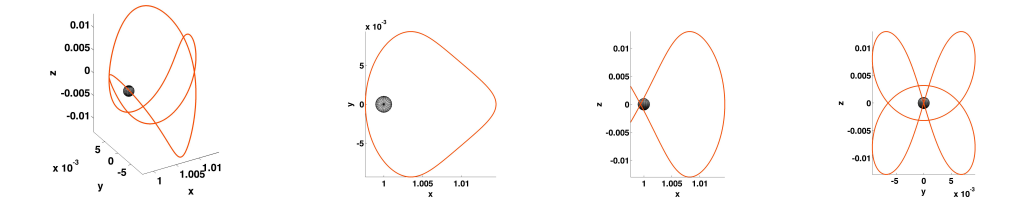

(i) P-2: C=3.002629675, T=4.9 (j) x-y (k) x-z (l) y-z, unstable

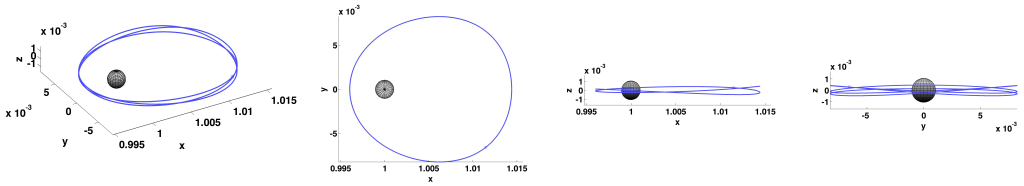

(m) P-3: C=3.003628817, T=4.87 (n) x-y (o) x-z (p) y-z, stable

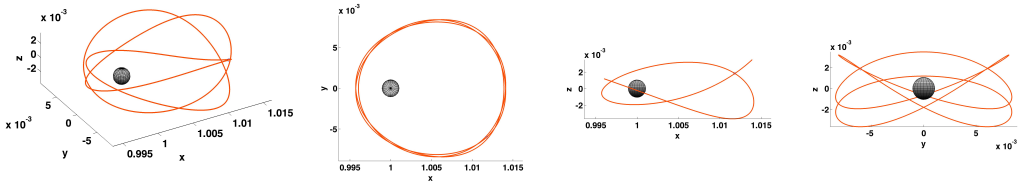

(q) P-3: C=3.003546469, T=4.937 (r) x-y (s) x-z (t) y-z, unstable

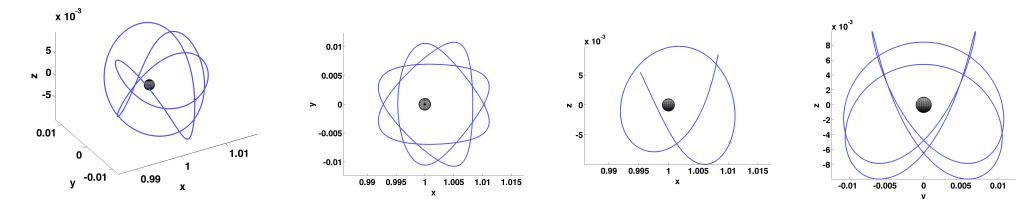

(u) P-3: C=3.002829006, T=5.7 (v) x-y (w) x-z (x) y-z, stable

Figure 11: H_2 P-2 and P-3 family of the J-E system

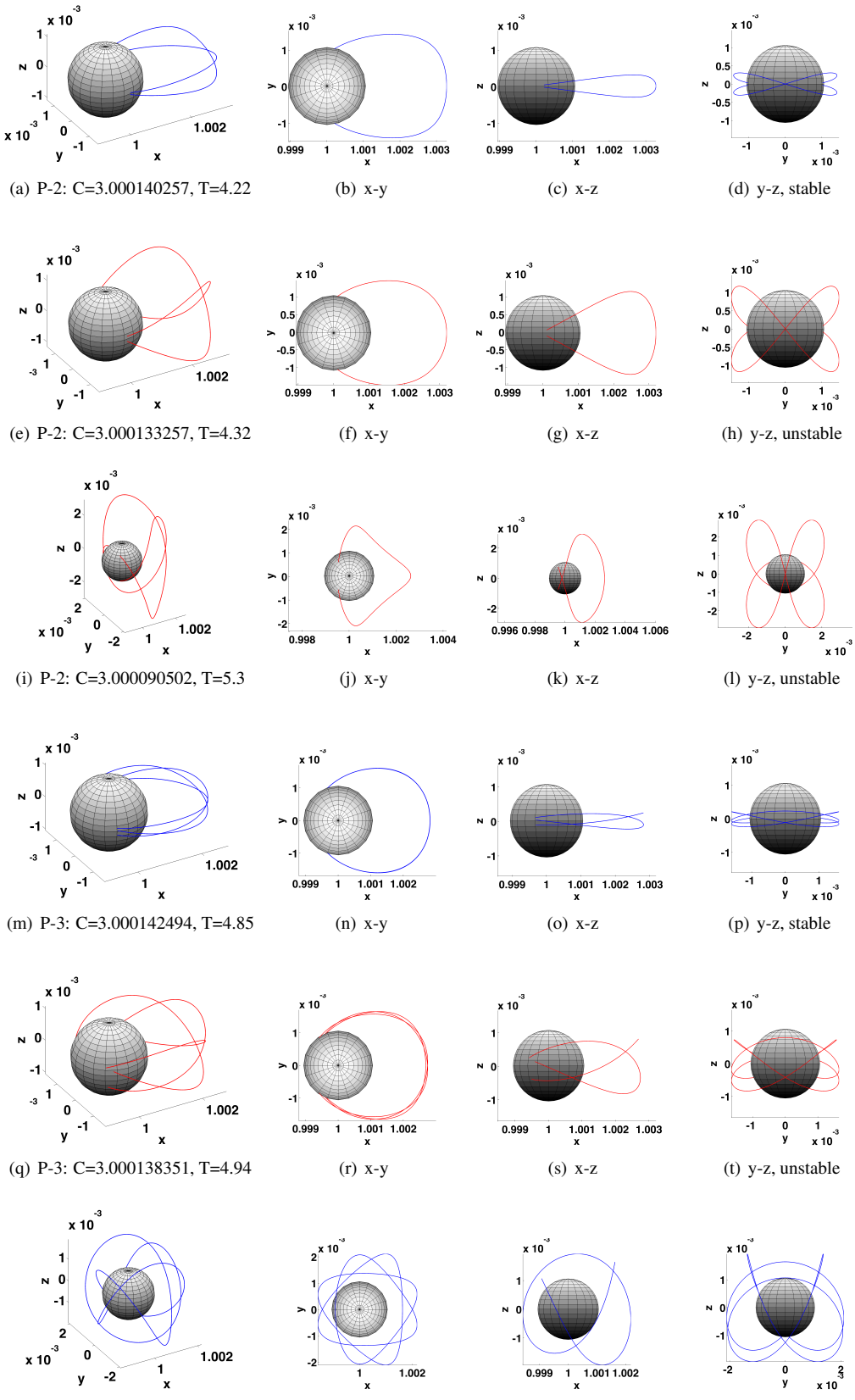

(a) P-2: C=3.000140257, T=4.22 (b) x-y (c) x-z (d) y-z, stable

(e) P-2: C=3.000133257, T=4.32 (f) x-y (g) x-z (h) y-z, unstable

(i) P-2: C=3.000090502, T=5.3 (j) x-y (k) x-z (l) y-z, unstable

(m) P-3: C=3.000142494, T=4.85 (n) x-y (o) x-z (p) y-z, stable

(q) P-3: C=3.000138351, T=4.94 (r) x-y (s) x-z (t) y-z, unstable

(u) P-3: C=3.000111747, T=5.7 (v) x-y (w) x-z (x) y-z, stable

Figure 12: H_2 P-2 and P-3 family of the S - E system

HIGHLY INCLINED ORBIT STUDY

Since the typical orbit search methods are based on symmetry, it is not possible to cover global behavior in a comprehensive manner. The cell-mapping method has been developed for generic orbits of generic systems not limited to symmetric constraints. Moreover, highly inclined orbit families are one of the interesting candidates for potential landing missions to guarantee decent visibility and communication opportunities. Various highly inclined orbits or asymmetric solutions for the Jupiter-Europa system were found using the cell-mapping method, and some of them are shown in Fig. 13.

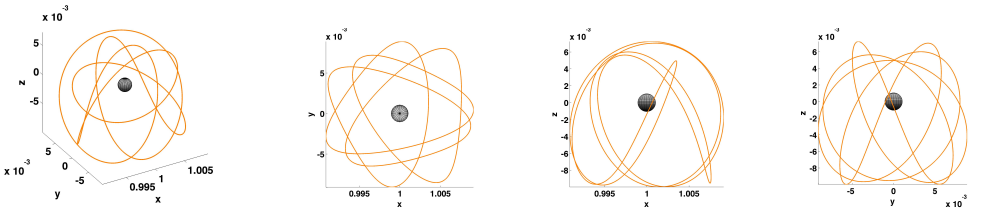

(a) C=3.00307721, T=5.7 (b) x-y (c) x-z (d) y-z, max λ=1.012843

(Initial condition: x,y,z,$\dot{x}$,$\dot{y}$,$\dot{z}$ = 1.000834274, -0.008094871, 0.000447792, 0.021269686, 0.024045627, 0.0446278)

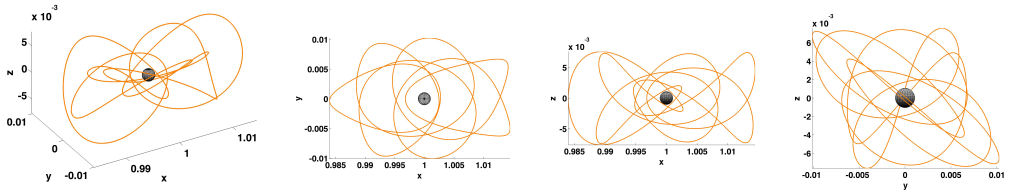

(e) C=3.00333913, T=9.8 (f) x-y (g) x-z (h) y-z,max λ=1.29559

(Initial condition: x,y,z,$\dot{x}$,$\dot{y}$,$\dot{z}$ = 0.987933813, -0.005947329, -0.013976278, -0.003537395, 0.004254574, 0.012897444)

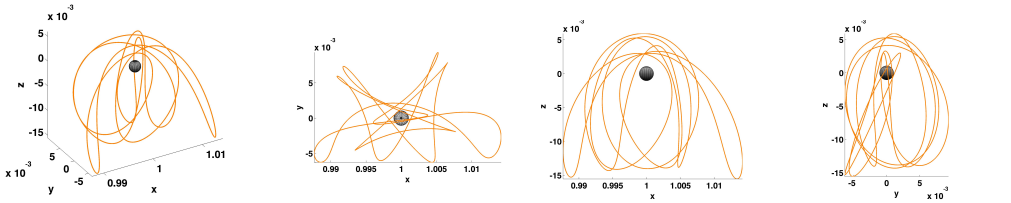

(i) C=3.00254373, T=8.9 (j) x-y (k) x-z (l) y-z, max λ=1.13498783

(initial condition: x,y,z,$\dot{x}$,$\dot{y}$,$\dot{z}$ = 1.001406423, 0.010198229, -0.006806296, -0.023222049, 0.00253405, 0.008261795)

Figure 13: Asymmetric orbits in J-E system

The first orbit family of Fig. 13 was continued in a Jacobi constant range from C=3.002756277 to C=3.003067835 for $5.7 < T < 6$, and it should be possible to continue it further. All the family members are fairly stable in this range with a maximum eigenvalue $\lambda \lesssim 1.01$. One of the continued orbits of Figs. 13a-13d can be found in Russell[27] (orbit ID=150541). The second orbit family of Fig. 13 is a part of a family from C = 3.003064266 to C = 3.003528899 with $9.44 < T < 10.45$. For $C \gtrsim 3.003388081$ and $T \lesssim 9.7$, orbits impact the surface of Europa. Because of its long period, several loops around the moon, and close approach to the moon, this orbit family can be an interesting option to study for a landing trajectory. Another interesting characteristic for this family is that there are planar orbit families that resemble it. There exist mirrored families with respect to the line x = 1-μ; one is stable and the other is unstable, but both sides are mostly impact orbits. The last orbit shown in Fig. 13 (Figs. 13i-13l), named 'Hat' in this paper, is studied in detail because of its interesting characteristics. The Hat family consists of highly inclined, asymmetric, long period orbits with a Jacobi constant range of C = 3.002186894 through C = 3.0026002491. Interestingly, a similar orbit family was found in the range of C = 3.002375528 through 3.00261845, but the family is

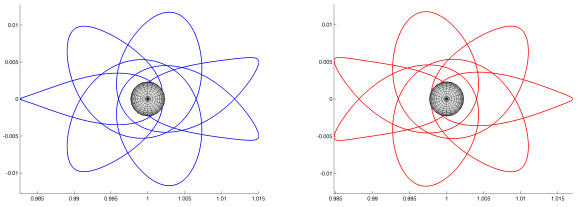

(a) λ_{max}=1.000, C=3.0037255 (b) λ_{max}=1.586, C=3.0037226

Figure 14: Planar orbit family of Figs.13e-13h, T = 8

marginally symmetric with respect to x = 1-μ. The two orbit families' properties are compared in Table 3. Hat_1 is more stable than the highly asymmetric Hat_2 family and one of the loops of Hat_1 impacts the surface of the moon under C = 3.00262085. The solutions are shown in Figs. 15 and 16. In summary, the Hat_1 and the Hat_2 families are presented in several different perspectives. Figure 17 shows that the Hat_1 family is closer to the surface and the Hat_2 bifurcates $r_p \approx 4e - 3$. Both families converge to $C \approx 3.0026$.

Table 3: Hat family orbits

name	C	T	maximum λ	property
Hat_1	3.002375528 – 3.002618451	8.7 – 9.4	1.8408 –1.0003	mostly impact the surface
Hat_2	3.002186894 – 3.002600249	8.54 – 9.2	72.3901 –1.0000	highly asymmetric

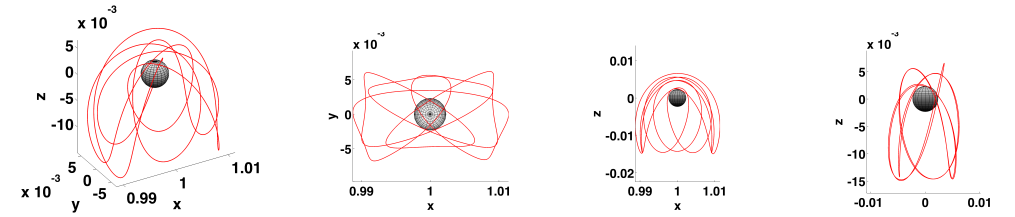

(a) Hat_1: C=3.002443247, T = 9.4 (b) x-y (c) x-z (d) y-z, λ_{max}=1.841

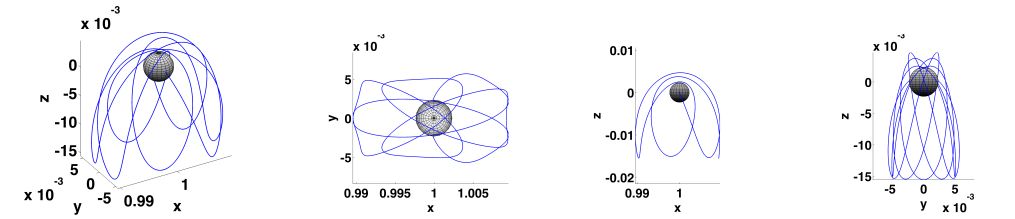

(e) Hat_1: C=3.002604695, T = 8.8 (f) x-y (g) x-z (h) y-z, λ_{max}=1.000

Figure 15: The Hat_1 family for J-E

Bifurcation of Three-Dimensional Orbits

One more orbit family, '$Loop_4$', was chosen to show its interesting features. The orbit family consists of two horizontally mirrored orbits. The orbits spend time dominantly on one side of the pole. North pole

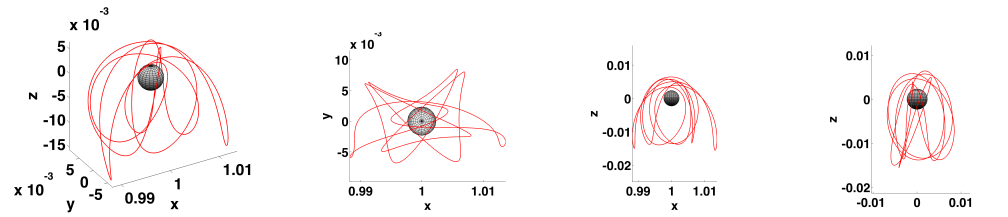

(a) Hat_2: C=3.00260512, T=9.29 (b) x-y (c) x-z (d) y-z, λ_{max}=9.139

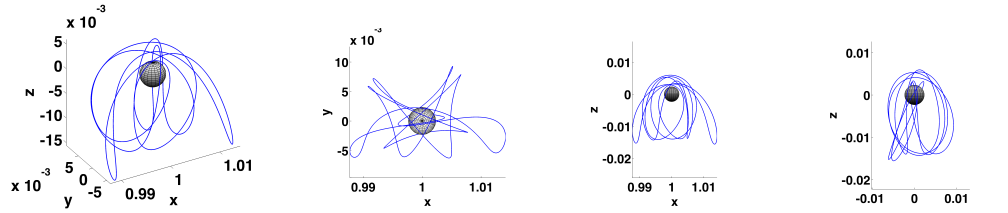

(e) Hat_2: C=3.00255379, T=8.93 (f) x-y (g) x-z (h) y-z, λ_{max}=1.000

Figure 16: The Hat_2 family for J-E

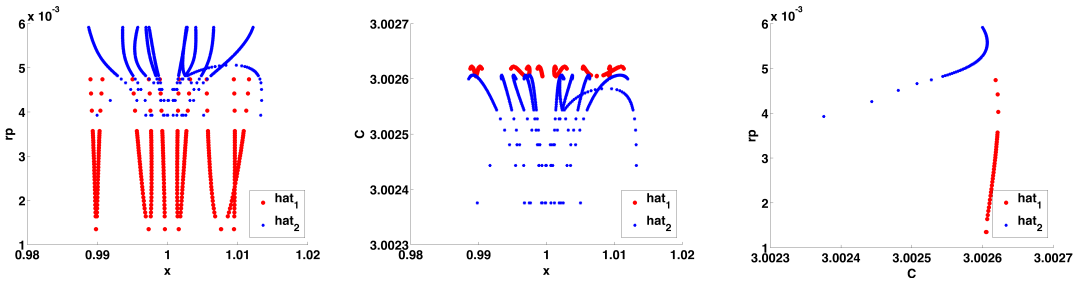

(a) x vs r_p (b) x vs C (c) C vs r_p

Figure 17: The Hat_1 and Hat_2 family transition for J-E

dominant orbits were selected for this paper. The selected fundamental $Loop_4$ P-1 family orbit between C = 3.00267570 and C = 3.00281431 is shown in Fig. 18. The $Loop_4$ P-1 is moderately stable, but period doubling is found when T $\approx$ 4.62 where C = 3.00280061. The $Loop_4$ P-2 orbits are plotted in Fig. 19 to show how the family bifurcates from the P-1 family. Eigenvalue analysis for the bifurcation is presented in Fig. 20. The horizontal line in Fig. 20b shows when the eigenvalue index is equal to λ = -2. The bifurcation diagrams were generated for x vs. the minimum distance from Europa to the orbit and x vs. C when y = 0 (see Fig. 21). Blue single lines represent $Loop_4$ P-1, and red double lines represent $Loop_4$ P-2 orbits. The period doubling bifurcation is shown fairly clearly in the bifurcation diagram.

CONCLUSIONS

In this paper, the cell-mapping method is applied to the Jupiter-Europa and the Saturn-Enceladus systems for the preliminary extensive orbit search study. Some well-known solutions, such as the H_2 family, were found for both systems, and their scale and characteristics were compared. A variety of orbit families were found using the cell-mapping method. Some of the periodic orbits from this method were confirmed with the previous studies proving the accuracy of the methodology. Various highly inclined and asymmetric orbits were also added to the orbit catalog, and these new orbits will be helpful to complete the global characteriza-

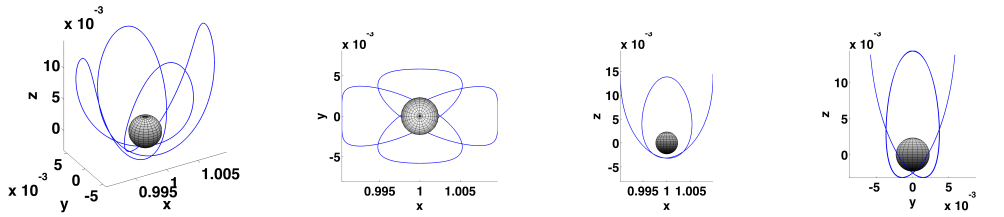

(a) P-1: C=3.00279735, T=4.6 (b) x-y (c) x-z (d) y-z, λ_{max}=1.795

Figure 18: Loop$_4$ P-1 orbits

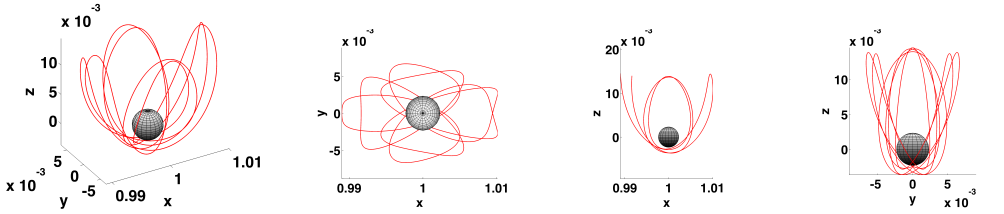

(a) P-2: C=3.002792633, T=9.2 (b) x-y (c) x-z (d) y-z, λ_{max}=3.296

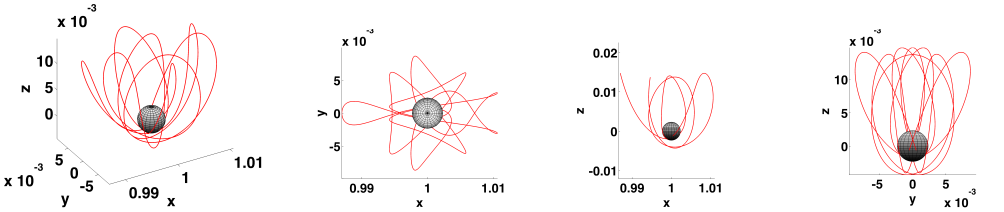

(e) P-2: C=3.00271719, T=9 (f) x-y (g) x-z (h) y-z, λ_{max}=3.929

Figure 19: Loop$_4$ P-2 orbits

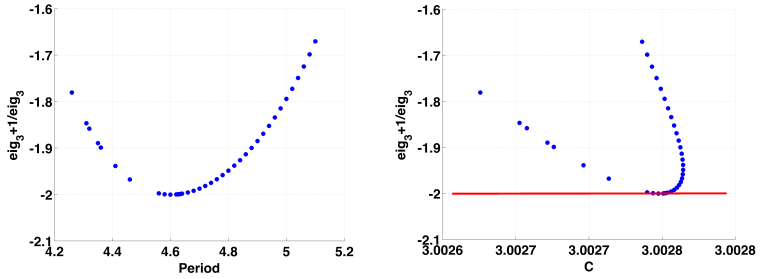

(a) Period vs eigenvalue index (b) C vs eigenvalue index

Figure 20: Eigenvalue index for Loop$_4$ bifurcation

tion of the behavior of the systems. Since the cell-mapping method can capture multiple-period of periodic solutions and global dynamics more completely, interesting bifurcation phenomena were also studied.

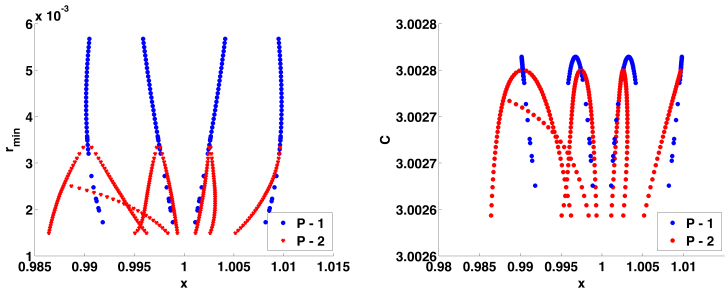

(a) x vs minimum distance (b) x vs C

Figure 21: Loop_4 bifurcation

ACKNOWLEDGMENT

Part of the research presented in this paper has been carried out at the Jet Propulsion Laboratory, California Institute of Technology, under a contract with the National Aeronautics and Space Administration. The High Performance Computing resources used in this investigation were provided by funding from the JPL Office of the Chief Information Officer. Copyright 2017 California Institute of Technology. U.S. Government sponsorship acknowledged.

REFERENCES

[1] Poincaré, H., New Methods of Celestial Mechanics (English Translation History of Modern Physics and Astronomy, American Institute of Physics, Vol. 13, 1993.

[2] Szebehely, V., Theory of Orbits-The Restricted Problem of Three Bodies. Academic Press, New York and London,1967. 443-449.

[3] Goudas, C. L., Three-Dimensional Periodic Orbits and Their Stability Icarus, Vol. 2, 1963. 1–18.

[4] Markellos, V.V., Numerical Investigation of the Planar Restricted Three-Body Problem. I. Periodic orbits of the second generation in the Sun-Jupiter System. Celes. Mech., Vol. 9, 1974. 365–380

[5] Zagouras, C. and Markellos, V. V., Axisymmetric Periodic Orbits of the Restricted Problem in Three Dimensions Astro. & Astrophys., Vol 59, 1977. 79–89.

[6] Robin, I. A. and Markellos, V. V., Numerical Determination of Three-Dimensional Periodic Orbits Generated from Vertical Self-Resonant Satellite Orbits Celestial Mechanics, Vol. 21, 1980. 395–434.

[7] Zagouras, C.G., Three-Dimensional Periodic Orbits about the Triangular Equilibrium Points of the Restricted Problem of Three Bodies Celestial Mechanics, Vol. 37, 1985. 27–46.

[8] Howell, K. C. and Pernicka, H. J., Numerical Determination of Lissajous Trajectories in the Restricted Three-Body Problem Celestial Mechanics, Vol. 41, 1988. 107–124.

[9] Hénon, M., Vertical Stability of Periodic Orbits in the Restricted Problem Astron. Astrophys., Vol. 28, 1973. 415–426.

[10] Message, P. J. On Asymmetric Periodic Solutions of the Plane Restricted Problem of Three Bodies G. E. O. Giacaglia (ed.), Periodic Orbits, Stability and Resonances, 1970. 19–32.

[11] Farquhar, R.W. and Kamel, A. A., Quasi-Periodic Orbits about the Translunar Libration Point Celestial Mechanics, Vol. 7, 1973. 458–473.

[12] Markellos, V. V., Black, W., and Moran, P. E., A Grid Search for Families of Periodic Orbits in the Restricted Problem of Three Bodies Celes. Mech., Vol. 9, 1974. 507–512.

[13] Kazantzis, P. G. and Goudas, C. L., A Grid Search for Three-Dimensional Motions and Three New Types of Such Motions Astrophysics and Space Science, Vol 32, 1975. 95-113.

[14] Markellos, V. V., Asymmetric Periodic Orbits in Three Dimensions Mon. Not. R. astr. Soc., Vol. 184, 1978. 273–281.

[15] Roy, A. E., and M. W. Ovenden., On the occurrence of commensurable mean motions in the solar system: the mirror theorem. Monthly Notices of the Royal Astronomical Society, 115.3, 1955. 296-309.

[16] Breakwell, J. V. and Brown, J. V., The Halo Family of 3-Dimensional Periodic Orbits in the Earth-Moon Restricted 3-Body Problem Celestial Mechanics, Vol. 20, 1979. 389-404.

[17] Howell, K. C., Three-dimensional, periodic, 'Halo' Orbits Celestial Mechanics, Vol. 32, No. 1, 1984. 53–71.

[18] Henon, M., New Families of Periodic Orbits in Hill's Problem of Three Bodies Celest. Mech. Dyn. Astr., Vol. 85, No. 3, 2003. 223–236.

[19] Tsirogiannis, G.A., Perdios, E.A., and Markellos, V.V., Improved Grid Search Method: an efficient tool for global computation of periodic orbits Celest. Mech. Dyn. Astr., Vol. 103, 2009. 49-78.

[20] Papadakis, K. E., Families of Asymmetric Periodic Orbits in the Restricted Three-Body Problem Earth Moon Planet, Vol. 103, 2008. 25–42.

[21] Farquhar, R.W., The Utilization of Halo Orbits in Advanced Lunar Operations NASA Technical Report, TN D-6365, 1971.

[22] Marchand, B. G., Howell, K. C., and Wilson, R., Improved Corrections Process for Constrained Trajectory Design in the n-Body Problem Journal of Spacecraft and Rockets, Vol. 44, No. 4, July-August, 2007. 884–497.

[23] Taylor, D. B., Families of Asymmetric Periodic Solutions of the Restricted Problem of Three Bodies for the Sun-Jupiter Mass Ratio and Their Relationship with the Symmetric Families Celestial Mechanics, Vol 29, 1983. 51–74.

[24] Dunham, D. W. and Farquhar, R. W., Libration point mission, 1978–2002 Libration Point Orbits and Applications: Proceedings of the Conference, Aiguablava, Spain, 10-14, June, 2002. 45–73.

[25] Hsu, C. S., A Theory of Cell-to-Cell Mapping Dynamical Systems. J. Applied Mechanics, Vol. 47, No. 4, 1980. December, 931–939.

[26] Hsu, C. S., An Unraveling Algorithm for Global Analysis of Dynamical Systems: An Application of Cell-to-Cell Mappings. J. Applied Mechanics, Vol. 47, No. 4, 1980. Dec. 940–948.

[27] Russell, R. P., Global Search for Planar and Three-Dimensional Periodic Orbits Near Europa The Journal of the Astronautical Sciences, Vol. 54, No. 2, April-June. 2006. 199–226.

[28] Dellnitz, M. and Junge, O., On the Approximation of Complicated Dynamical Behavior SIAM Journal on Numerical Analysis, Vol. 36, No. 2, 1999. 491–515.

[29] Dellnitz, M. and Froyland, G. and Junge, O., The algorithms behind GAIO – Set oriented numerical methods for dynamical systems Ergodic Theory, Analysis, and Efficient Simulation of Dynamical Systems, Springer, Fiedler, B. 2001. 145–174

[30] Dellnitz, M. and Junge, O., Set Oriented Numerical Methods in Space Mission Design Modern Astrodynamics, Elsevier Astrodynamics Series, Butterworth-Heinemann. 2006.

[31] Wang, F. and Lever, P., A cell mapping method for general optimum trajectory planning of multiple robotic arms Robotics and Autonomous Systems, Vol. 12, 1994. 15–27

[32] Koh, D. and Flashner, H., Global Analysis of Gravity Gradient Satellite's Pitch Motion in an Elliptic Orbit Journal of Computational and Nonlinear Dynamics, Vol. 10, No. 6, 2015. 061020

[33] Koh, D. and Anderson, R. L., Periodic orbit-attitude solutions in the planar elliptic restricted three-body problem AIAA/AAS Astrodynamics specialist conference, Long Beach, CA, September, 13-16, 2016. ASD-36 2490399.

[34] Ding, Q., Cooper, J.E., and Leung, A.Y.T., Application of an improved cell mapping method to bilinear stiffness aeroelastic systems Journal of Fluids and Structures, Vol. 20, 2005. 35–49.

[35] Pini, A. J., B. F. Villac, and R. L. Anderson, From Simplified to Complex Small-Body Models: Sensitivity Analysis of Periodic Orbit Sets 27th AAS/AIAA Space Flight Mechanics Meeting, AAS 17-371, American Astronautical Society, San Antonio, Texas, February 5-9, 2017.

[36] Villac, B. F., Anderson, R. L., and Pini, A. J., Computer Aided Ballistic Orbit Classification Around Small Bodies The Journal of the Astronautical Sciences, Volume 63, Number 3, 2016. 175–205.

[37] Lunine, I. J., Ocean Worlds Exploration Acta Astronautica, Vol. 131, 2017. 123–130.

[38] Koh, D., Periodic motion analysis in spacecraft attitude dynamics Ph.D. Thesis, University Southern California, May, 2016.

[39] Flashner, H., and Hsu, C. S., A Study of Nonlinear Periodic Systems via the Point Mapping Method International Journal for Numerical Methods in Engineering, Vol. 19, No. 2, 1983. 185–215.

[40] Guttalu, R. S., and Flashner, H., Stability Analysis of Periodic Systems by Truncated Point Mapping Journal of Sound and Vibration, Vol. 189, No. 1, 1996. 33–54.

[41] Parker, J. S., and Anderson, R. L., Low-energy lunar trajectory design John Wiley & Sons, 2014.

[42] Broucke, R. A., Periodic Orbits in the Restricted Three-Body Problem With Earth-Moon Masses Jet Propulsion Laboratory, Technical Report 32-1168, February 15, 1968.